Microfabricated Transition-Edge X-ray Detectors

G. C. Hilton, John M. Martinis, K. D. Irwin, N. F. Bergren, D. A. Wollman,
M. E. Huber, S. Deiker, and S. W. Nam

***Abstract*— We are developing high performance x-ray detectors based on superconducting transition-edge sensors (TES) for application in materials analysis and astronomy. Using our recently developed fully lithographic TES fabrication process, we have made devices with an energy resolution of 4.5 $\pm$0.1 eV for 5.9 keV x-rays, the best reported energy resolution for any energy dispersive detectors in this energy range. These detectors utilize micromachined thermal isolation structures and transition-edge sensors fabricated from Mo/Cu bilayers with normal-metal boundary conditions. We have found the normal-metal boundary conditions to be critical to stable and reproducible low noise operation. In this paper we present details of fabrication and performance of these devices.**

Index Terms— **X-ray detectors, IR detectors, microcalorimeter, x-ray spectrometry**

I. Introduction

Microcalorimeters utilizing superconducting transition-edge sensors (TES) are an important new class of x-ray detectors. Such detectors [1] have obtained energy resolutions as good as 2 eV for 1.5 keV x-ray photons with count rates as high as 500 s^{-1}. The performance of TES microcalorimeters make them applicable to a wide variety of applications in both materials analysis and x-ray astronomy. In addition, these detectors are electrically compatible with recently developed superconducting quantum interference device (SQUID) based multiplexers [2], potentially enabling the development of large pixel-count arrays of TES microcalorimeter x-ray detectors. In fact, many of the potential applications of TES microcalorimeters require the extension of the single pixel results described here to arrays of thousands of pixels.

X-ray microcalorimeters consist of three basics functional units: an absorber of incident radiation to convert the x-ray energy into thermal energy, a thermometer that measures the temperature rise of the microcalorimeter, and a thermal isolation structure that controls the escape of heat from the device. Absorbers are fabricated from materials with short x-ray absorption lengths and thermalization times compatible with the detector speed. We have typically utilized thick (2 μm) Bi films as absorbers. A variety of different thermometers have been employed in cryogenic microcalorimeters including Si thermistors [3], NTD Ge thermistors [4], [5] and transition edge sensors [6]. Transition edge sensors have two significant advantages over other thermometers, high sensitivity $\alpha = d\ \log R/d\ \log T$, and fast response time due to negative electrothermal feedback [7]. Our TES's are made from proximity-effect coupled normal-superconductor bilayers. Using these bilayers we are able to obtain a tunable superconducting critical temperature, T_c, in the desired range near 100 mK while maintaining the low resistivity necessary for fast thermal response. Thermal isolation of our detectors is provided by either micromachined low-stress Si_3N_4 membranes or micromachined Si legs made using a silicon-on-insulator process.

Until recently [8], fabrication of our TES microcalorimeters detectors was performed by shadow-mask methods. Individual chips with free standing silicon nitride membranes are mounted in an electron-beam evaporator in which the Al/Ag bilayer, Al wiring, Ag bias resistor, and Bi absorber are evaporated through shadow masks. While we have obtained excellent results with this method [1], the use of shadow-masks severely limits device geometries and likely precludes the fabrication of large arrays of detectors.

II. Bilayer Development

While Al/Ag proved to be a good bilayer for our shadow-mask detectors, this material system is unsuitable for microfabricated detectors because of rapid electrochemical and thermal degradation under standard processing conditions. It was necessary to find an improved material system. Given the constraints of low normal resistance, the normal layer of the bilayer must be one of the noble metals, Au, Ag or Cu. The superconducting layer must then be a superconductor with T_c greater than 100 mK and less than roughly 2 K, and both chemically and thermally compatible with the noble metals. Of the possible choices, we felt that Mo [9] was the most promising. Molybdenum is widely used in semiconductor and superconductor fabrication processes; it is essentially insoluble with the noble metals [10] and has a very low rate of oxide formation. The latter property is important in the formation of bilayers where any oxide barrier has a significant effect on the reproducibility of bilayer T_c through the interface transmission factor t [11]. Others have made bilayers using Ir [12] or Ti [13]. Iridium is both difficult to deposit and has a T_c that is too low (0.112 K) for many potential applications of TES-based detectors. Titanium forms (albeit at high temperature) many intermetallic phases with all the noble metals, and rapidly forms oxide barriers.

Unlike the Mo/Au bilayers demonstrated by Finkbeiner *et al.* [9], which were fabricated using electron beam evaporation of Mo onto heated substrates($> 500\,^{\circ}$C), we chose to deposit Mo by sputtering onto room temperature substrates. The low deposition temperature allows us to immediately deposit the

Manuscript received September 19, 2000. This work supported in part by NASA. Contribution of U.S. Government, not subject to copyright.

The authors are with the National Institute of Standards and Technology, Boulder, CO 80303, USA (email:*hilton@boulder.nist.gov*) except M. E. Huber who is with the Department of Physics, University of Colorado at Denver, Denver, CO 80217, USA

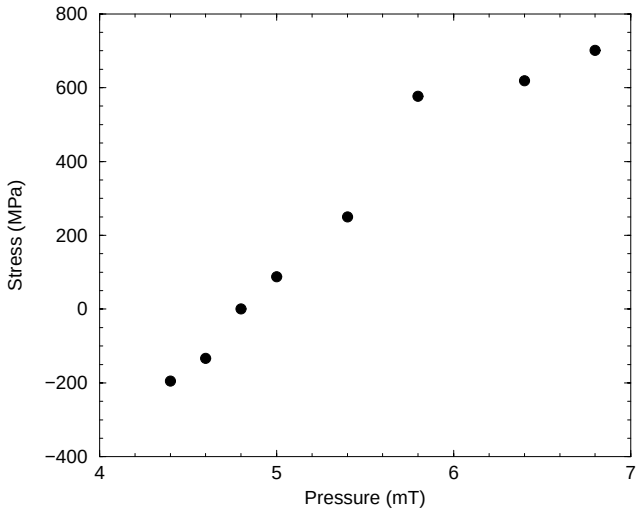

Fig. 1. Stress in 150 nm thick sputtered Mo films as a function of Ar pressure. Positive (negative) values indicates tensile (compressive) stress.

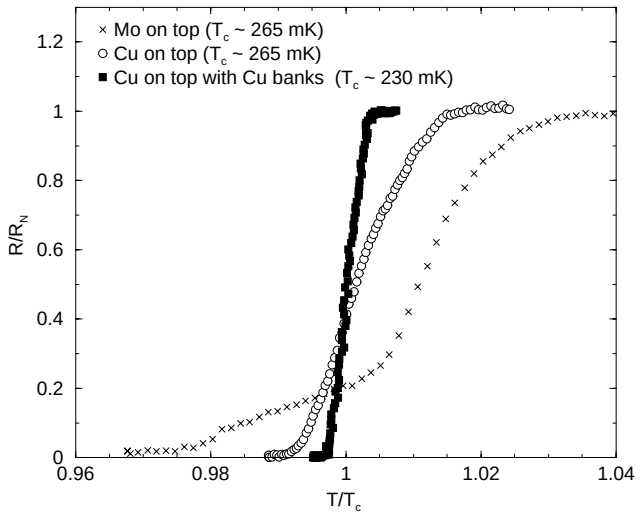

Fig. 2. Superconducting transitions for 30 square 4-terminal samples of microfabricated bilayers in various configurations. The plots have been normalized in both resistance and temperature for ease of comparison.

normal metal without a long in-vacuum cooling process, possibly leading to cleaner bilayer interfaces. Additionally, our process may permit future integration of bilayer TES devices with existing SQUID fabrication to allow for the integration of read-out electronics.

Before attempting to make bilayers, we optimized the Mo deposition parameters for superconducting performance. The sputtering target consisted of 99.992% pure vacuum melted Mo and was mounted in a 75 mm diameter DC magnetron in a sputter-up configuration with the substrates mounted 110 mm from the target. The sputtering power is fixed at 200 W. Because the TES detector will ultimately be fabricated on a free standing micromachined structure, it is imperative to obtain low stress bilayer films. As is typical of refractory metals, it is possible to obtain highly stressed films, and the sputtering pressure must be carefully adjusted to achieve low stress films. In Fig. 1 we show such an optimization for Mo films. For materials with low stress (less than roughly 100 MPa) we find essentially no variation in electrical properties. Our low stress Mo films have a T_c of 1.05 K - somewhat higher than the bulk value of 0.915 K, a resistivity at room temperature of between 9 and 10 $\mu\Omega$-cm, roughly twice the bulk value of 5.2 $\mu\Omega$-cm, and a RRR of 1.9. We have also found that the above parameters are only achieved when the film is patterned by etching. When pattern the film using a lift-off technique we obtain much higher and variable transition temperatures, presumably due to contamination from the photoresist. A similar optimization was carried out for all three possible normal metals. Because the most important parameter for the normal metal is low resistivity at the TES operating temperature, we chose the film with the highest RRR, Cu. The film was sputtered using a 99.999 % pure Cu target. We typically obtain a room temperature resistivity of 2.1 $\mu\Omega$-cm, somewhat greater than the bulk value of 1.7 $\mu\Omega$-cm. For a 200 nm thick Cu film we obtain a RRR of 8.

Bilayers containing these two metals were then fabricated in a variety of configurations. The use of lift-off was quickly abandoned after the adverse effects on the Mo T_c were found. A variety of etchants for both layers were identified. The Mo was found to be easily etched either using an SF_6 plasma or a standard Al "PAWN"etch (H_3PO_4:CH_3COOH:H_20:HNO_3 16:1:2:1 by volume). The Cu films were etched using a commercially prepared $(NH_4)_2S_2O_8$ based copper etchant, which was found to have the smallest undercut of all tested etchants.

Test structures consisting of TES bilayers were patterned in a four-terminal geometry with widths of 100 μm and 300 μm and a length of 3 mm (30 and 10 squares respectively). The superconducting transitions of test structures fabricated in three different configurations are plotted in Fig. 2. In the first two cases the films were patterned with a somewhat wider normal metal layer in order to prevent shorting out the bilayer by any superconducting film left on the outer edges of the test device. In both of these cases we obtain somewhat disappointing results. The superconducting transitions are relatively wide and show undesirable structure. We attribute this to imperfections along the edge of the test structures. If the normal metal and superconductor do not achieve intimate contact along the outer edges of the TES, the reduced proximity coupling of the two layers will lead to a somewhat higher local T_c. The decoupling of the films at the edges could occur through chemical degradation of either of the two films or at their interface, or through a physical effect such as stress-induced delamination.

We solve these difficulties by adding a strip of normal metal to the outer edge of the TES in a separate processing step. A schematic of the resultant structure is shown in Fig. 3. The bilayer is deposited by first sputtering the Mo layer and then the Cu layer in rapid succession. We then pattern both the Cu and Mo layers by wet etching. Within the TES, the Mo is patterned to be several micrometers wider than the Cu. The

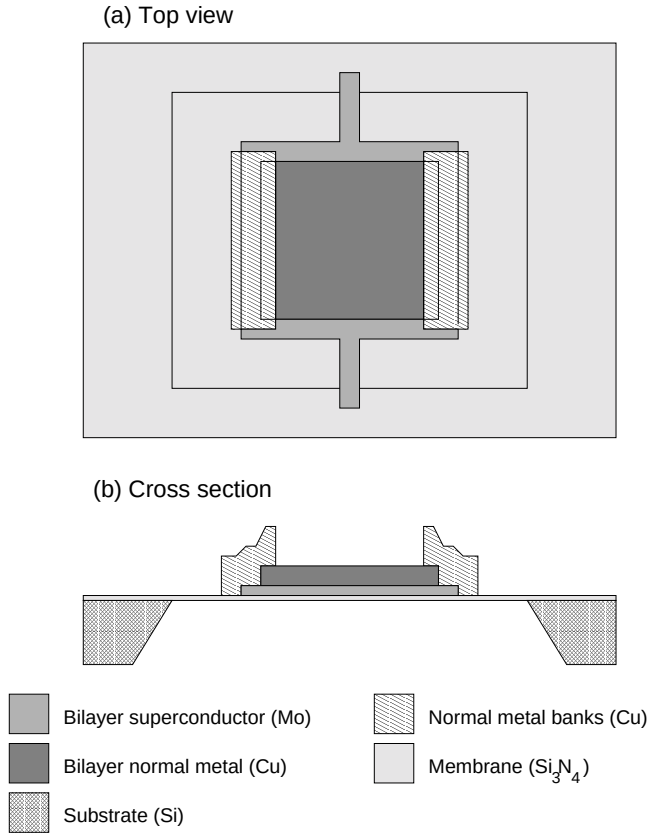

Fig. 3. Schematic layout (not to scale) of bilayer and normal bank geometry showing (a) the top view of the device and (b) a cross section through the center portion.

additional normal metal strips or "banks" are then added by evaporating a layer of Cu through a photoresist lift-off stencil. The interface between the bilayer and the banks is cleaned prior to deposition by RF sputter etching with Ar^+. The Cu bank is made much thicker than the normal metal of the bilayer and extends both 3 μm to 5 μm onto normal metal of the bilayer and 3 μm to 5 μm beyond the outer edge of the TES. The resulting transition, shown in Fig. 2, is narrow and free from artifacts. The banks assure that there is normal metal on the edge of the TES and that the Cu/Mo interfaces are buried away from possible chemical degradation.

TES test structures of several Mo and Cu thicknesses were fabricated and measured to obtain the interface transmission factor t=0.39. With this factor we can calculate the T_c of an arbitrary TES design using equation (9) in [11]. Our nominal design for x-ray microcalorimeter TES detectors consists of 66 nm of Mo and 200 nm of Cu with 500 nm thick Cu normal banks. With these parameters we typically obtain a T_c of 100 mK and a resistance of 15 m$\Omega/\Box$. In order to assure adequate proximity coupling between the Mo and the bank, we also measured the transmission factor obtained between Mo and Cu deposited by the bank process. The measured transmission varies between 0.25 and 0.35, indicating that the 500 nm bank will fully supress superconductivity at the TES edges.

III. Fabrication Details

The above described bilayer fabrication process must be integrated into a membrane micromachining process in order to yield complete detectors. We start with 75 mm diameter, 250 μm thick <100>, double-side-polished Si wafers. These wafers have a 250 nm thick low-pressure chemical vapor deposition coating of low-stress (Si rich) Si_3N_4 on both sides. The Si_3N_4 will eventually become the thermal isolation membrane. In order to align the backside micromachining etch steps to the front side TES detector structures it is necessary to place registered alignment marks on front and back sides of the wafer. A 150 nm thick Al layer is deposited on the front side and patterned using a wet etch (PAWN at 50°C) to give front-side alignment marks. The aluminum is also left as a protective layer covering the portion of the device that will become the free standing membrane. Prior to the use of this protective coating a slight over-etch in a subsequent reactive-ion-etch (RIE) step was found to substantially increase the chance of membrane failure. Registered back-side alignment marks are then patterned on the wafer using an IR transmission alignment tool. These alignment marks are etched into the back-side silicon nitride using a parallel-plate plasma etcher with a 2:1 CF_4:O_2 gas mixture.

Utilizing the back-side alignment marks, windows for the micromachining step are patterned and etched using the same procedure as the back-side alignment marks. The wafer is then placed in an etching apparatus that uses silicone o-rings to protect the front side of the wafer. The wafer is etched using a commercial buffered KOH anisotropic Si etch formulation at 95 °C. Roughly 200 μm of the wafer are removed at this step. Performing the bulk of the Si etch before TES deposition eliminates thermal exposure of the TES device during this step, while leaving 50 μm of Si under the membrane, maintaining a strong wafer capable of withstanding normal wafer handling. The depth of the KOH etch is periodically monitored by measuring the horizontal length of the Si (111) plane exposed by the etch. With this procedure we can compensate for the variable KOH etch rate.

A wiring layer of 200 nm thick Nb is then deposited on the front side. This layer is primarily used to make contact with the detector bias resistor. The Nb layer is patterned using a sloped sidewall reactive ion etch (RIE) recipe utilizing CHF_3 and O_2. The remaining protective Al over the membrane area is now stripped using the same etching procedure used for the front-side alignment marks.

The device is now ready for the fabrication of the bilayer TES and normal banks as described in the previous section. After fabrication of the TES, a lift-off stencil consisting of 3 μm thick negative photoresist is applied before deposition of the Bi absorber. The TES is lightly cleaned before deposition of the absorber to improve thermal contact. The 2 μm thick Bi absorber is deposited using electron-beam deposition. After lift-off, a layer of positive photoresist is applied and patterned with the "fly-swatter" (Fig. 4) pattern used to etch the nitride membrane. The wafer is then again mounted in the back-side

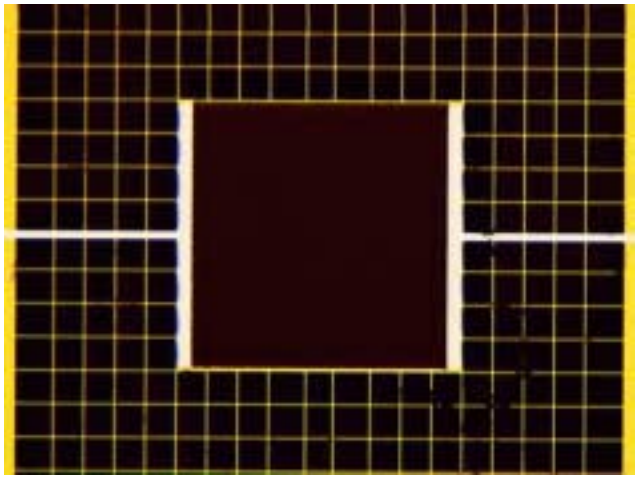

Fig. 4. Optical micrograph of TES microcalorimeter showing fly-swatter membrane structure, Bi absorber covering the 400 μm $\times$ 400 μm TES. The legs of the fly-swatter are 3 μm wide. Superconducting Mo leads exit to the left and right of the detectors

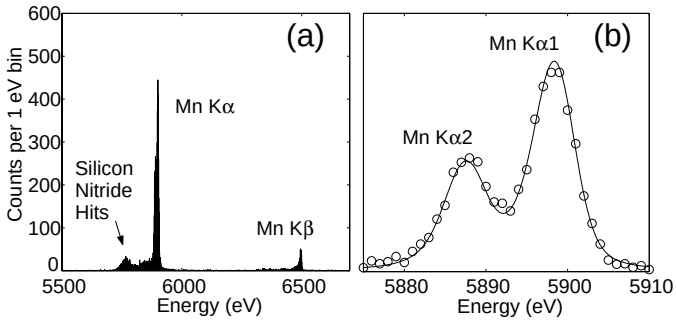

Fig. 5. (a) Energy spectra for ^{55}Fe x-rays using a microfabricated TES microcalorimeter. Because this device did not have a Bi absorber, additional low energy events are visible which are attributed to x-rays absorbed in the Si_3N_4 membranes. (b) The measured energy spectra (circles) and a fit (solid line) yielding an energy resolution of 4.5 $\pm$ 0.1 eV for the Mn K_α x-rays at 5.9 keV

etching apparatus and the same KOH-based etching solution at 95 °C is used to remove the remaining Si in the membrane area leaving only the membrane. After removal from the etching jig the wafer is diced into chips. The individual nitride membranes of these chips are then etched using a CHF_3 and O_2 RIE etch. The flyswatter photoresist mask is then removed using a plasma ashing step. A photograph of such a completed device is shown in Fig. 4. Note that the TES microcalorimeter is only supported by a sparse mesh of Si_3N_4 legs.

IV. Results and Conclusions

The performance of devices fabricated using this process has been measured. The devices are mounted on a cold finger in a two-stage adiabatic demagnetization refrigerator to provide cooling, and connected to a two-stage SQUID preamplifier. A detailed decription of the measurement procedure and performance details is presented elsewhere [8]. Our best measured x-ray spectrum obtained when such a detector is illuminated with x-rays from an ^{55}Fe source is plotted in Fig. 5. The detector used to acquire this data did not include a Bi absorber. When this spectra is fit against the measured Mn $K_{\alpha1}$ and Mn $K_{\alpha2}$ line profiles we obtain a Gaussian instrument resolution of 4.5 $\pm$ 0.1 eV full width at half maximum for the 5.9 keV Mn K_α x-rays [8]. The resolving power for this detector ($E/\Delta E \approx$ 1300) is the best reported for any microcalorimeter to date.

We have developed a robust fabrication process that has produced the highest performing microcalorimeters yet reported. This process utilizes standard materials and processes and is likely to be compatible with future integration of additional superconducting preamplifiers or multiplexing electronics. The TES portion of this process is compatible with the necessary scaling of these single detector results to many pixel arrays, and should be compatible with the micromachining techniques proposed for obtaining large format arrays of close-packed pixels.

References

[1] D. A. Wollman, S. W. Nam, Dale E Newbury, G. C. Hilton, K. D. Irwin, N. F. Bergren, S. Deiker, D. A. Rudman, and John M. Martinis, "Superconducting transition-edge-microcalorimeter x-ray spectrometer with 2eV energy resolution at 1.5 keV," *Nucl. Instr. Meth. A*, vol. 444, pp. 145–150, 2000.

[2] J. A. Chervenak, K. D. Irwin, E. N. Grossman, John M. Martinis, C. D. Reintsema, and M. E. Huber, "Superconducting multiplexer for arrays of transition edge sensors," *Appl. Phys. Lett.*, vol. 74, pp. 4043–5, 1999.

[3] C. K. Stahle, R. L. Kelley, D. McCammon, S. H. Moseley, and A. E. Szymkowiak, "Microcalorimeter arrays for high resolution soft X-ray spectroscopy," *Nucl. Instrum. Meth. Phys Rsch. A*, vol. 370, pp. 173, 1996.

[4] E. Silver, M. Legros, G. Austin, and N. Madden, "First Use of NTD Germanium-Based Microcalorimeters for High-Resolution, Broad Band X-Ray Microanalysis," *X-ray Spectrometry*, vol. 25, pp. 265–268, 9 1997.

[5] A. Alessandrello, J. W. Beeman, C. Brofferio, O. Cremonesi, E. Fiorini, A. Giuliani, E. E. Haller, A. Monfardini, A. Nucciotti, M. Pavan, G. Pessina, E. Previtali, and L. Zanotti, "High Energy Resolution Bolometers for Nuclear Physics and X-Ray Spectroscopy," *Phys. Rev. Lett.*, vol. 82, pp. 513–515, 1999.

[6] K. D. Irwin, "An application of electrothermal feedback for high resolution cryogenic particle detection," *Appl. Phys. Lett.*, vol. 66, pp. 1998–2000, 1995.

[7] K. D. Irwin, G. C. Hilton, D. A. Wollman, and John M. Martinis, "Thermal-response time of superconducting transition-edge microcalorimeters," *J. Appl. Phys.*, vol. 83, pp. 3978–3985, Apr. 1998.

[8] K. D. Irwin, G. C. Hilton, John M. Martinis, S. Deiker, N. Bergren, S. W. Nam, D. A. Rudman, and D. A. Wollman, "A Mo-Cu superconducting transition-edge microcalorimeter with 4.5 eV energy resolution at 6 KeV," *Nucl. Instr. Meth. A*, vol. 444, pp. 184–187, 2000.

[9] F. M. Finkbeiner, T. C. Chen, S. Aslam, E. Figueroa-Feliciano, R. L. Kelley, M. Li, D. B. Mott, C. K. Stahle, and C. M. Stahle, "Fabrication of Superconducting Bilayer Transistion Edge Thermometers and their Application for Spaceborne X-ray Microcalorimetry," *IEEE Transactions on Applied Superconductivity*, vol. 9, pp. 2940–42, June 1999.

[10] Thaddeus B. Massalski, Ed., *Binary Alloy Phase Diagrams, Second Edition*, ASM International, 1990.

[11] John M. Martinis, G. C. Hilton, K. D. Irwin, and D. A. Wollman, "Calculation of T_c in normal-superconductor bilayer using the microscopic-based Usadel theory," *Nucl. Instr. Meth. A*, vol. 444, pp. 23–27, 2000.

[12] Hohne J., Altmann M., Angloher G., Hettl P., Jochum J., Nussle T., Pfnur S., Schnagl J., Sarsa M. L., Wanninger S., and Von Feilitzsch F., "High-resolution x-ray spectrometry using iridium-gold phase transition thermometers," *X-ray Spectrometry*, vol. 28, pp. 396–398, 9 1999.

[13] H. F. C. Hoevers, A. C. Bento, M. P. Bruijn, L. Gottardi, M. A. N. Korevaar, W. A. Mels, and P. A. J. de Korte, "Performance of a microcalorimeter with a superconducting transition edge thermometer," *Nucl. Instrum. Meth. A*, vol. 444, pp. 192–195, 2000.